Microchimica Acta (2019) 186:490
https://doi.org/10.1007/s00604-019-3589-0

ORIGINAL PAPER

Photoelectrochemical determination of trypsin by using an indium tin oxide electrode modified with a composite prepared from MoS_2 nanosheets and TiO_2 nanorods

Weisu Kong[1] · Qin Li[1] · Lian Xia[1] · Xiaomeng Li[1] · Han Sun[1] · Rong-Mei Kong[1] · Fengli Qu[1]

Received: 28 February 2019 / Accepted: 6 June 2019

Abstract

A photoelectrochemical (PEC) method has been developed for sensitive detection of trypsin. It is based on the use of a composite consisting of MoS_2 nanosheets and TiO_2 nanorods (MoS_2-TiO_2). The material has a high specific surface area, superior electrical conductivity, excellent biocompatibility and good band gap matching. The composite was synthesized by a one-pot method using TiO_2 as a template. This results in a uniform distribution of the MoS_2 nanosheets (<5 layers) in the composite. If the composite, placed on an indium tin oxide (ITO) electrode, is coupled to apoferritin, the photocurrent response decreases due to the insulating effect of the protein. Trypsin, in acting as an alkaline protease, decomposes the apoferritin. This results in the recovery of the PEC signal. Attractive features of this PEC method include (a) a superior PEC signal, (b) sensor stability, (c) simple operation, and (d) the lack of any additional modifications of the biosensor. This warrants high sensitivity, reproducibility, repeatability and practicality. The ITO sensor has a linear response in the 1 to 1000 ng·mL^{-1} trypsin concentration range and a 0.82 ng·mL^{-1} detection limit. The assay was applied to the determination of trypsin in spiked serum samples and gave satisfactory results.

Keywords Photoelectrochemical assay · MoS_2 nanosheets · TiO_2 nanorods · Trypsin · Apoferritin

Introduction

Trypsin is the most important digestive enzyme produced by trypsinogen. It plays an important role in regulating pancreatic exocrine function [1]. A large number of diseases are associated with changes in trypsin levels, such as pancreatitis, vesicular fibrosis and carcer [2–4]. To date, a variety of techniques have been established for trypsin detection, such as colorimetric assay [5], electrochemical methods [6], fluorescence [7], and inductively coupled plasma mass spectrometry [8]. Despite the advances have been made in this field, the clinical detection are still restricted by the low sensitivity, complex operation and expensive equipment. There are still many challenges for developing simple, fast and low cost strategies for the detection of trypsin.

Photoelectrochemical (PEC) biosensing of antigens, enzymes, enzyme substrates and other biomarkers has been intensively investigated because of the fast response, low-cost measurement, low background and high sensitivity [9]. PEC detection has potential advantages and an excitation source (photocurrent) with complete separation and different energy forms, which can reduce the background signal [10]. Photoactive materials with superior PEC properties are the key component for constructing biosensors with good analytical performances. The coupling of small bandgap semiconductors with large bandgap semiconductors can strengthen charge separation by suppressing electron-hole recombination, which leads to amplification of photocurrent generation [11]. Therefore, it is of great importance to develop stable, low-cost semiconductors with good biocompatibility and proper band alignment for PEC systems to generate photocurrent efficiently.

Titanium dioxide (TiO_2) has been considered as a promising photocatalyst due to its inexpensive properties, high specific surface area, strong optical

Electronic supplementary material The online version of this article (https://doi.org/10.1007/s00604-019-3589-0) contains supplementary material, which is available to authorized users.

✉ Rong-Mei Kong
kongrongmei@126.com

✉ Fengli Qu
fengliquhn@hotmail.com

[1] College of Chemistry and Chemical Engineering, Qufu Normal University, Qufu, Shandong 273165, People's Republic of China

Published online: 02 July 2019

absorption, favorable band edge position and sufficient availability [12, 13]. However, the higher electron-hole recombination rate and wider optical band gap (about 3.2 eV) make the photocurrent conversion efficiency of TiO_2 still limited [14]. Certain methods have been developed to increase its photoelectric conversion efficiency, including dye sensitization [15], quantum dots deposition [16], metal and non-metal atom doping [17], and semiconductor coupling [18]. It has been reported that coupling TiO_2 nanomaterials with other narrow-bandgap semiconductors to form nanocomposites can effectively improve the photoconversion efficiency [19]. For example, a Co_3O_4-CNT hybrid TiO_2 composite was successfully utilized for the construction of glucose aptamer sensors [20]. The light conversion efficiency of visible light activity on the composite modified sensor was improved due to the small energy gap of Co_3O_4. TiO_2-$CuInS_2$ core-shell structure also exhibited high photocatalytic activity for photoelectrochemical water degradation [21], which was due to the close matching of the optimal band gap of $CuInS_2$ and TiO_2 with a higher absorption coefficient.

As a two-dimensional layered material, MoS_2 is a semiconductor belonging to a class of compounds called layered transition metal dichalcogenides [22]. Structurally, the Mo atom is sandwiched between two S atomic layers by interacting through a weak van der Waals. In addition, MoS_2 has a high charge mobility, large specific surface area and excellent photoelectron conversion performance, which is widely used in the fields of photocatalysis and hydrogen production [23, 24]. Compared with zero dimensional nanoparticles that are only in point contact, the structure of the layered junction increases the contact area of effective charge transfer across the interface, shortens the charge transfer time and distance, thereby promoting the separation of electron-hole pairs and improving photoconversion efficiency [25]. Most importantly, MoS_2 has a layered structure similar to that of graphite and can be peeled off into a single layer or several layers of nanosheets, and can adjust the inherent band gap by changing the number of layers [26]. In particular, the band edge position of TiO_2 matches well with that of MoS_2 nanosheets, which was beneficial to the transfer of photogenerated charges and the improvement of separation efficiency [27].

Herein, the TiO_2 nanorod was prepared using a hydrothermal method, which functionalized as templates to synthesize MoS_2 nanosheets-TiO_2 nanorods (MoS_2-TiO_2) composites by a one-pot method. The composites had large specific surface area, excellent electrical conductivity and good band gap matching. In particular, with the template of TiO_2 nanorod, the synthesis of the composites was controlled and the distribution of the MoS_2 nanosheet (<5 layer) in the composites was stable and uniform. The PEC signal of the MoS_2-TiO_2 composites was 6 times higher than that of TiO_2 nanorods alone. After immobilizing the MoS_2-TiO_2 composites on the surface of the ITO electrode, the apoferritin (APO) was adsorbed, which resulted in the photocurrent response was severely suppressed to 20% of the original data due to the insulating effect of the protein. The presence of trypsin can efficiently decompose the APO, resulting in the recovery of the photocurrent intensity. The photocurrent intensity was proportional to the amount of trypsin. The PEC biosensors had a linear range of 1 to 1000 $ng{\cdot}mL^{-1}$ for the detection of trypsin, and the detection limit was 0.82 $ng{\cdot}mL^{-1}$.

This effective on-off-on biosensor presented a reliable protease detection strategy with simple operation, low background signal, and good sensitivity. The sensor platform provides high sensitivity and a wide range of options for trypsin detection, with great potential for high-throughput protease assay applications. The unique strategy for trypsin detection in human serum samples was conducted with satisfactory results, suggesting its potential application for diagnostic purposes.

Experimental section

Reagents and materials

Titanium tetrachloride ($TiCl_4$) was purchased from Kermel, (Tianjin, China, http://www.chemreagent.com). Chloroform ($CHCl_3$) and acetone were ordered from Fuyu Fine Chemical (Tianjin, China, http://ccn.mofcom.gov.cn/915596/). Sodium molybdate dihydrate ($Na_2MoO_4{\cdot}2H_2O$), bovine serum albumin (BSA), urea, and human serum albumin (HSA) were supplied from Aladdin Chemical (Shanghai, China, http://www.aladdin-e.com). Thiourea and absolute ethanol were purchased from Sinopharm Chemical (Shanghai, China, http://www.sino-reagent.com). Apoferritin (APO), glucose (GL), glucose oxidase (GOx), α-amylase (α-AM) and trypsin were purchased from Sigma-Aldrich (USA, https://www.sigmaaldrich.com). Phosphate buffer saline (PBS, 0.1 M, pH 7.8) was applied for trypsin incubation and PEC detection. All reagents were analytical grade and used directly. The solutions were prepared with deionized water.

Apparatus

The morphology, internal structure and composition of the prepared material were observed by a scanning electron microscope (SEM: JSM-6700F) and transmission electron microscope (TEM: JEM-2100). The X-ray diffraction (XRD) pattern was determined using a MiniFlex600 (Rjgaku Co. Japan). X-ray photoelectron

spectroscopy (XPS) spectra was obtained from an ESCALAB 250Xi spectrometer (Thermo Fisher, USA) with a light intensity of 300 W cm^{-2} estimated by a radiometer (Ceaulight Corporation, China). All the experiments were measured on a CHI 660E electrochemical workstation (Shanghai Chenhua Instrument Co., China) with a three-electrode system. A modified MoS_2-TiO_2 photoanode with a geometric square area (1.0 ± 0.1 cm^2) was the working electrode, a Pt wire was the counter electrode, and a saturated Ag/AgCl electrode was the reference electrode.

Photoelectrochemical (PEC) biosensor fabrication

Indium tin oxide (ITO) glass substrate treatment: ultrasonic cleaning with ethanol, acetone and deionized water, drying at 50 °C for 3 h. 10 μg·mL^{-1} trypsin solution was prepared in 0.1 M PBS buffer (pH 7.8). The ITO electrode was modified with MoS_2-TiO_2 (ITO/MoS_2-TiO_2) by drop-coating in 10 μL of MoS_2-TiO_2 solution (1 mg·mL^{-1}). After drying, 10 μL of APO (1 mg·mL^{-1}) solution was coated on an ITO/MoS_2-TiO_2 electrode and dried at 50 °C for 3 h to ensure effective fixation of APO. The ITO/MoS_2-TiO_2/APO electrode was thoroughly rinsed with 0.1 M PBS buffer and dried naturally at room temperature for further use.

PEC detection of trypsin

The PEC measurement was conducted by using a three-electrode system which comprised with a material modified ITO electrode saturated Ag/AgCl and platinum wire as a working electrode, a reference electrode and an auxiliary electrode, respectively. A potential of + 0.4 V (vs. Ag/AgCl) was applied to the working electrode using a CHI 660E electrochemical workstation to record photocurrent. PBS buffer containing various concentrations of trypsin with a final volume of 30 mL was used as test solution. The Xe lamps with a spectral range of 200–2500 nm are excitation sources that turn on and off every 20 s. The length between ITO and visible light is 10 cm.

Results and discussion

Choice of materials

The TiO_2 has nontoxic, inexpensive properties, high specific surface area, excellent biocompatibility, strong optical absorption and favorable band edge position [12, 13]. MoS_2, layered transition metal dichalcogenides, has large specific surface area, high charge mobility and excellent photoelectron conversion property [23, 24]. Furthermore, TiO_2 nanorods have good matching with the edge positions of MoS_2 nanosheets, which was beneficial to the transfer of photogenerated charges [27].

The mechanism of the sensing scheme

The sensing mechanism of the sensing platform is illustrated in Scheme 1. MoS_2-TiO_2 composites with high PEC signal were synthesized successfully by a one-pot method using TiO_2 as a template, which were modified on the ITO electrode by drop-coating method. The PEC signal was dramatically decreased after the effective immobilization of APO on the ITO/MoS_2-TiO_2 because of the insulating effect of the protein. Trypsin catalytically hydrolyzed APO specifically and induced the PEC signal recovery. A simple and sensitive PEC platform for trypsin detection was constructed as the trypsin activity was positive correlation to the decreased PEC signal. In addition, the electron-hole separation and transport mechanism of MoS_2-TiO_2 is shown in the inset illustration of Scheme 1. As indicated by the dashed lines, the conduction band (CB) level of the bulk or multilayer MoS_2 is lower than that of TiO_2, so electrons cannot be injected into the TiO_2 from MoS_2 [28]. Furthermore, changing the thickness of MoS_2 can adjust the band gap of MoS_2 [29]. The S-Mo-S layer is composed of bulk MoS_2 through van der Waals interconnect, and the indirect band gap is 1.2 eV. More importantly, as the number of layers decreases, the band gap of MoS_2 increases gradually because of the quantum confinement effect [30]. With irradiation, electrons in the valence band (VB) of MoS_2 are excited to the CB to generate electron-hole pairs. Then, the photoelectrons are rapidly injected into the CB of the TiO_2 nanorods and transferred to the ITO to obtain a photocurrent. It is worth noting that the excited holes from the TiO_2 nanorods can jump back to the VB of MoS_2. Therefore, the photocurrent of MoS_2-TiO_2 composites increases, and the PEC signal can be realized.

Characterization of the MoS_2-TiO_2 composites

Figure 1 shows an XRD pattern of MoS_2, TiO_2 and MoS_2-TiO_2 composites. Separate MoS_2 (curve a) exhibits different diffraction peaks at 14.38°, 32.68° and 58.33°, which can be attributed to the (002), (100) and (110) crystal faces of MoS_2 [31]. In addition, the curve b shows eleven peaks at 27.45°, 36.09°, 39.19°, 41.23°, 44.05°, 54.32°, 56.64°, 62.74°, 64.04° and 69.01°, corresponding to (110), (101), (200), (111), (210), (211), (220), (002), (310) and (301) crystal plane reflection of rutile TiO_2 [32]. In the case of MoS_2-TiO_2 composites, all diffraction peaks of rutile TiO_2 are still present, suggesting that the MoS_2 nanosheets loading has no impact on

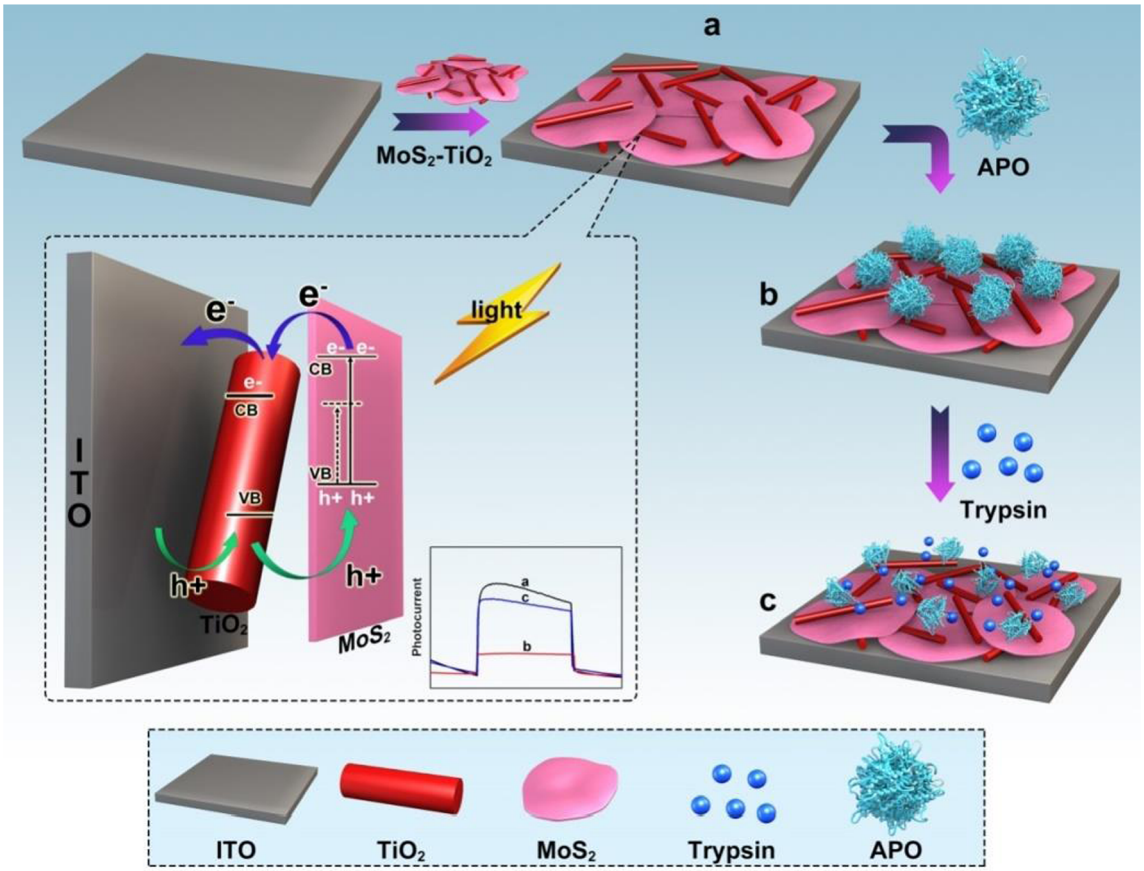

Scheme 1 Schematic illustration of PEC detection of trypsin based on MoS_2-TiO_2 composites and separation mechanism of photogenerated electron hole pairs of MoS_2-TiO_2 composite

the crystal phase of TiO_2. In curve c, three peaks are observed corresponding to the (002), (100) and (110) crystal faces of MoS_2, demonstrating the successful synthesis of MoS_2-TiO_2 nanomaterials. Furthermore, the MoS_2 diffraction peak at 14.38° in curve c is much weaker than in curve a. This is attributed to the fact that the formation of TiO_2 and MoS_2 composites are very beneficial to the generation of few layer nanostructures for MoS_2 [33].

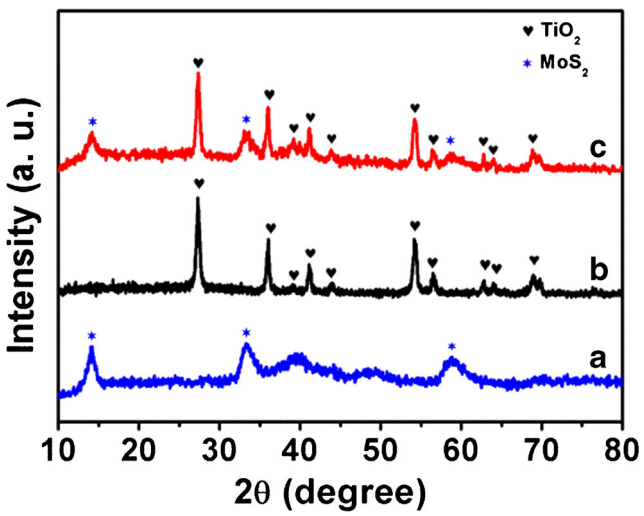

Fig. 1 XRD pattern of (**a**) pure MoS_2, (**b**) TiO_2 nanorod and (**c**) MoS_2-TiO_2 composite

SEM and TEM were utilized to acquire the features of TiO_2, MoS_2, and MoS_2-TiO_2 composites. Figure 2a displays the TEM and high-resolution TEM (HRTEM) images of pure TiO_2 nanorod with the average diameter of ~ 20 nm and length of ~ 180 nm. The HRTEM image in Fig. 2a inset shows that the interplanar spacing of TiO_2 nanorod is 0.325 nm, corresponding to the (110) plane of TiO_2. The TEM image of MoS_2-TiO_2 composite (Fig. 2b) shows that the ultra-thin MoS_2 nanosheets are combined with TiO_2 nanorods, indicating the successful preparation of MoS_2-TiO_2 composites. HRTEM image of MoS_2-TiO_2 composite (Fig. 2c) shows a well-resolved lattice fringe spacing with interplanar distances of 0.61 nm, corresponding to the (002) plane of MoS_2. The crystal plane results are coincident with Fig. 1. In the hydrothermal reaction process, TiO_2 nanorods were used as growth templates to prevent the re-stacking of MoS_2, and the TiO_2-MoS_2 composites were successfully synthesized [34]. As shown in Fig. 2d, pure MoS_2 microspheres are prepared using a synthetic procedure similar to the complex.

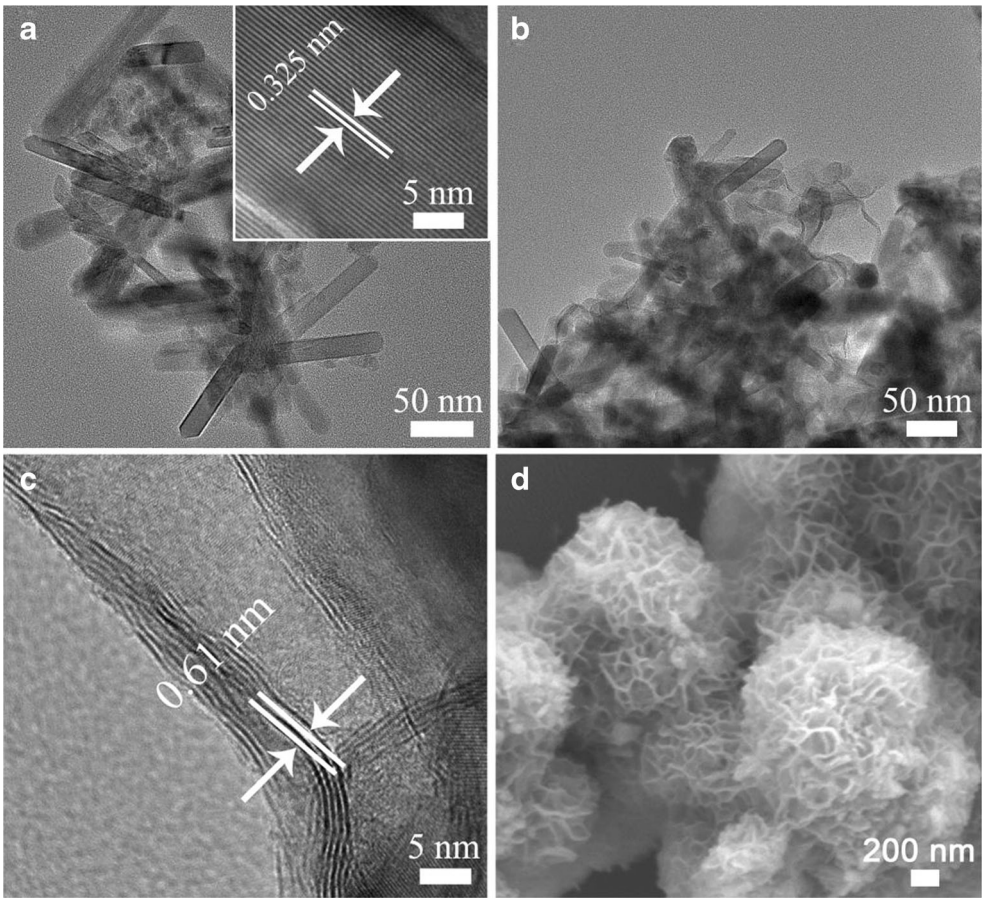

Fig. 2 TEM images of (**a**) TiO_2 nanorods, the inset plots is the HRTEM image of TiO_2 nanorods; (**b**) MoS_2-TiO_2 composite; (**c**) HRTEM images of MoS_2 in MoS_2-TiO_2 composite; SEM images of (**d**) MoS_2 micropheres

HRTEM image of MoS_2-TiO_2 composite (Fig. 2c) definitely illustrates that thin MoS_2 nanosheets are less than 5 layers after MoS_2 and TiO_2 composite. The SEM and TEM images demonstrate that pure MoS_2 is a flower-like microsphere, but forms less than five-layer nanostructure after compounding with TiO_2 nanorods.

As shown in Fig. 3a, the XPS survey spectrum of the MoS_2-TiO_2 composites suggest the existence of Mo, S, O, and Ti elements, demonstrating the successful synthesis of MoS_2-TiO_2 composite. As shown in Fig. 3b and Fig. 3c, four peaks are observed at 464.6, 458.9, 531.6, and 530.0 eV, which can be attributed to Ti $2p_{1/2}$, Ti $2p_{3/2}$ and Ti-OH groups on the surface of TiO_2 nanorods [32]. Figure 3d illustrates the high-resolution XPS spectra of Mo 3d which contains Mo $3d_{3/2}$ at 232.0 eV and Mo $3d_{5/2}$ at 228.9 eV. The peak at 226.1 eV actually corresponds to the S 2 s of MoS_2. In addition, the peaks at binding energies of 163.0 eV and 161.8 eV are observed (Fig. 3e), which are attributed to the S $2p_{1/2}$ and S $2p_{3/2}$ for the MoS_2, respectively [34]. The XPS measurements confirmed that the layered MoS_2 was successfully supported on the surface of TiO_2.

PEC and EIS characterizations

To further investigate the step-by-step manufacturing process, the interface properties of the electrode was characterized by PEC measurements and electrochemical impedance spectroscopy (EIS) (Fig. 4a, b). The PEC characteristics of the nanomaterials were characterized using the photocurrent generated by irradiating the modified ITO electrode with intermittently visible light. As shown in Fig. 4a, the ITO/TiO_2 electrode and ITO/MoS_2 electrode (curve i and curve ii) all shows the minimum photocurrents of 2.4 μA and 0.4 μA respectively as the absorption of visible light for the TiO_2 nanorods and MoS_2 nanosheets is weak. As expected, the photocurrent of the MoS_2-TiO_2 composites-modified ITO electrode (curve iii) is ~ 6 times that of the TiO_2 nanorods-modified ITO electrode (curve i). The matching band level enhances absorption of visible light and separation of charge due to the close interfacial contact between the MoS_2 nanosheets and the TiO_2 nanorods. The following incubation with the APO resulted in a significant decrease of the photocurrent (curve iv) due to the insulating effect of the protein.

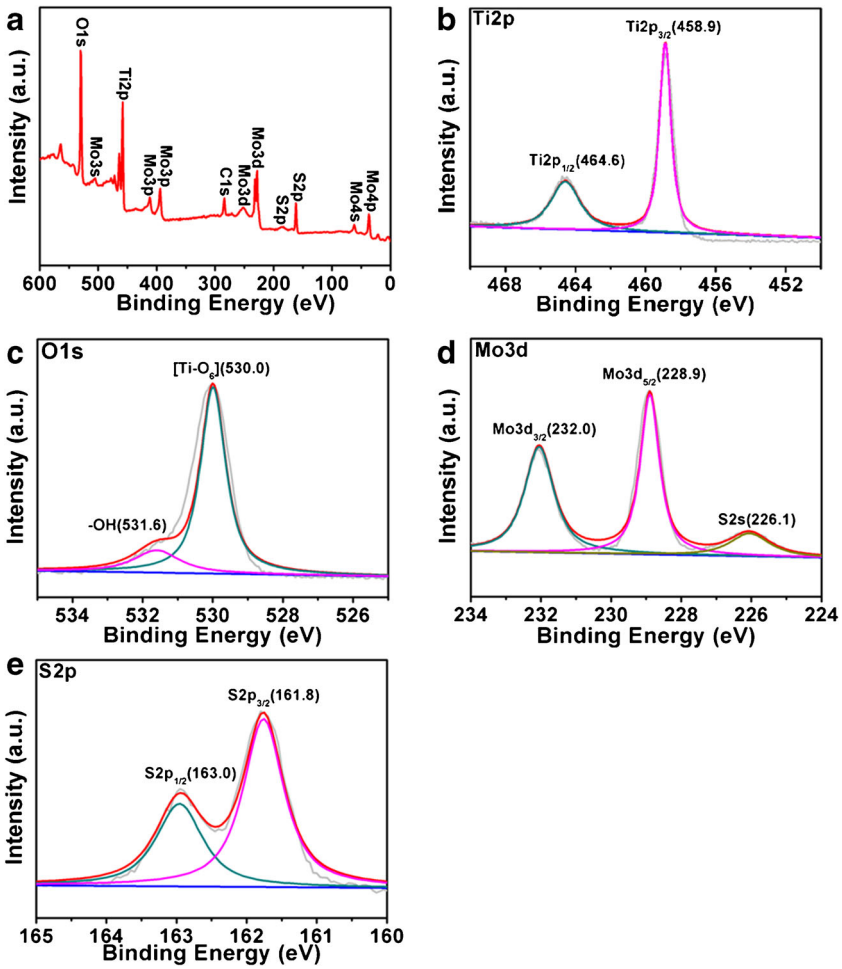

Fig. 3 XPS survey scans of (a) MoS_2-TiO_2 composites; High-resolution XPS spectra of (**b**) Ti 2p, (**c**) O 1 s, (**d**) Mo 3d, and (**e**) S 2p

However, after the cleavage of APO by trypsin, the photocurrent is obviously increased (curve v).

As shown in Fig. 4b, each EIS consists of a semicircular and linear portion of the reaction electron transfer and diffusion limited process. EIS Nyquist plots of MoS_2-TiO_2 (curve iii) presents a relatively lower electron-transfer resistance (Ret) compared with the pure TiO_2 (curve i) and pure MoS_2 (curve ii) as a result of strong conductivity of the composite material. This is attributed to the rapid electron transfer caused by the close interfacial contact between TiO_2 and MoS_2. When the APO is immobilized on the surface of the ITO/MoS_2-TiO_2 electrode, the Ret gradually increases due to the insulation of the protein molecule (curve iv). The trypsin specifically catalyzes the hydrolysis of APO after the ITO/MoS_2-TiO_2-APO electrode is incubated with the trypsin solution, resulting in the electron-transfer resistance and the Ret value decreased (curve v). This result also confirms the feasibility of PEC biosensors for trypsin detection.

Performance of the biosensor

The constructed sensing platform was applied to investigate the activity of trypsin under optimal conditions (See the Electronic Supplementary Material for specific optimization), which can be expressed sensitively by the degree of photocurrent change. As shown in Fig. 4c, the photocurrent signal increases as the increasing amount of trypsin linearly with the logarithm of trypsin concentrations from 1 to 1000 ng·mL^{-1} (Fig. 4d). The regression equation is $A = 5.66 + 0.84\log C_{trypsin}$, and the correlation coefficient is 0.995. The detection limit is 0.82 ng·mL^{-1} at S/N of 3. It is worth mentioning that the detection range and the LOD of the MoS_2-TiO_2 PEC biosensor are superior compared to other previous reports, which are given in Table S1 in the electronic supplementary material.

To investigate the selectivity of the biosensor towards trypsin, the photocurrent response was evaluated against other common substances such as BSA, HSA, GOx, α-AM, GL, urea and the corresponding mixture (Mix) with trypsin. As can be seen from Fig. 5, the photocurrent responses caused by the interfering substancescan be neglectable. Only the presence of trypsin triggers a significant photocurrent response, no matter the trypsin is alone or in the mixture. Such a high specificity can be attributed to the specific enzymatic catalysis reaction between APO and trypsin.

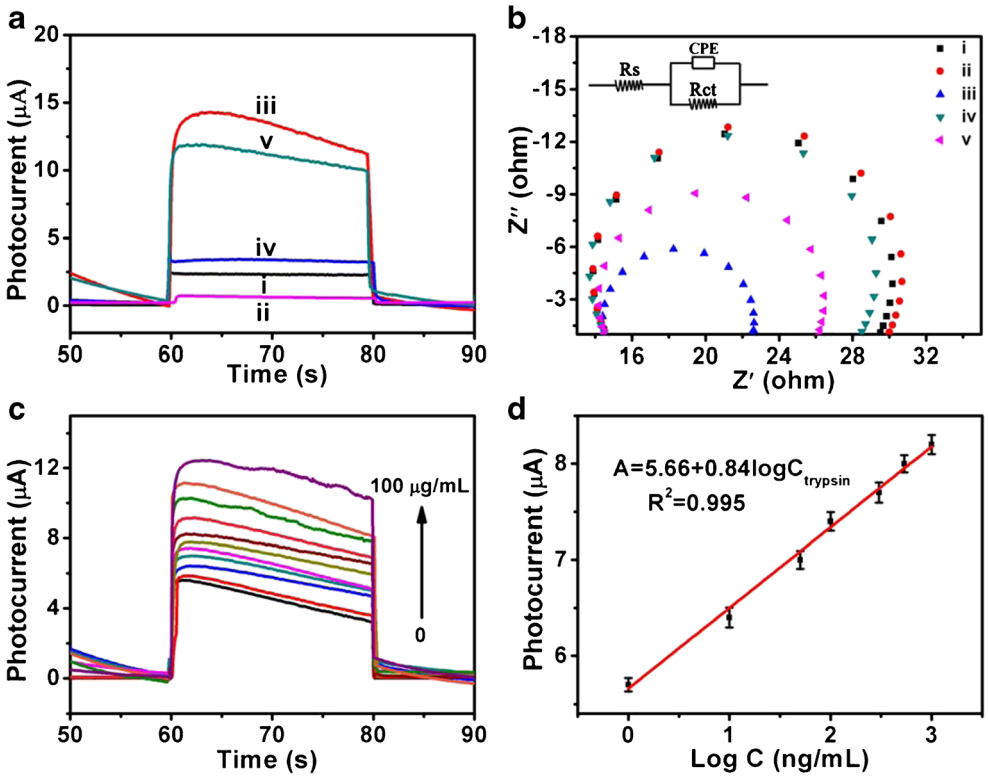

Fig. 4 (**a**) Photocurrent responses in 0.1 M PBS buffer (pH 7.8), and (**b**) EIS spectra in 5.0 mM $[Fe(CN)_6]^{3-/4-}$ (i) TiO_2|ITO; (ii) MoS_2|ITO; (iii) MoS_2-TiO_2|ITO; (iv) MoS_2-TiO_2-APO|ITO; (v) MoS_2-TiO_2-APO|ITO incubated with trypsin (10 μg·mL^{-1}). (**c**) Photocurrent responses of the different concentration of trypsin at + 0.4 V (vs. Ag/AgCl) (0.1, 1, 10, 50, 100, 300, 1×10^3, 3×10^3, 5×10^3, 7×10^3 and 1×10^4 ng·mL^{-1}, respectively). (**d**) The calibration plot with error bars with the standard deviation of three replicate determinations at a bias potential of + 0.4 V (vs. Ag/AgCl)

Detection of trypsin in serum samples

Common concentration of trypsin in healthy human serum is 4.1–7.4 ng·mL^{-1} [35]. To demonstrate the potential application of the trypsin assay in clinical diagnosis, the assay for trypsin detection in healthy human serum samples was performed. The serum was provided by the Qufu Normal University School Hospital. The trypsin content in the samples was derived from the calibration plot and the regression equation. The average recovery test was performed using standard addition methods and relative standard deviation (RSD). Specifically, a serum sample diluted 100 times was added into PBS buffer for 30 min at 40 °C to measure the PEC signal. Different concentrations of trypsin were added in the above solution, which was incubated for 30 min to detect the PEC signal. It can be seen that the recoveries of the serum samples are found to be in the range 98–104.3% from Table S2, which are satisfactory for quantitative assays performed in biological samples.

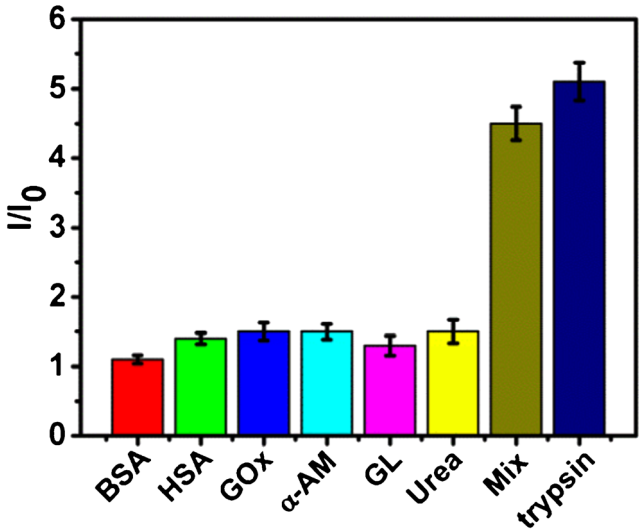

Fig. 5 Selectivity of the trypsin PEC sensor. The trypsin concentration, 10 μg·mL^{-1}; the concentrations of BSA, HSA, GOx, α-AM, GL, Mix, and Urea are all 10 μg·mL^{-1}. The PEC measurements were recorded in a bias potential of + 0.4 V (vs. Ag/AgCl). The error bars were derived from the standard deviation of five measurements. Error bar = SD (n = 5)

Conclusion

MoS_2-TiO_2 composites with high PEC signal were successfully prepared in one pot using TiO_2 nanostructures as growth templates to prevent re-stacking of MoS_2 nanosheets. The photocurrent response of the composite was significantly reduced by the incubation of APO due to the insulating effect of the protein. Trypsin enzymatically catalyzed APO hydrolysis specifically, which decomposed the APO and induced the PEC signal recovery. A simple, fast, low cost and sensitive PEC platform for trypsin detection was constructed as the trypsin activity was positive correlation to the increased PEC

signal. The stability and compatibility of the MoS_2-TiO_2 composites, along with the simple operations and no additional modification procedure ensured the excellent analytical performances of the trypsin biosensor. The biosensor allowed the detection of trypsin in the range of 1 ng·mL^{-1} to 1000 ng·mL^{-1} with a detection limit of 0.82 ng·mL^{-1}. The unique strategy was conducted in human serum samples for trypsin detection with satisfactory result. This strategy is the simplest PEC method for trypsin detection up to now to our best knowledge, revealing its potential applications in clinical testing.

Acknowledgements This work was supported by the National Natural Science Foundation of China (21775089, 21505084), Outstanding Youth Foundation of Shandong Province (ZR2017JL010), the Natural Science Foundation Projects of Shandong Province (ZR2017QB008), and the Key Research and Development Program of Jining City (2018ZDGH032).

Compliance with ethical standards The author(s) declare that they have no competing interests.

References

1. Hirota M, Ohmuraya M, Baba H, Gastroenterol J (2006) The role of trypsin, trypsin inhibitor, and trypsin receptor in the onset and aggravation of pancreatitis. J Gastroenterol 41:832–836
2. Zhang L, Du J (2016) A sensitive and label-free trypsin colorimetric sensor with cytochrome c as a substrate. Biosens Bioelectron 79: 347–352
3. Turk B (2006) Targeting proteases: successes, failures and future prospects. Nat Rev Drug Discov 5:785–799
4. Yamamoto H, Iku S, Adachi Y, Imsumran A, Taniguchi H, Nosho K, Min Y, Horiuchi S, Yoshida M, Itoh F, Imai K (2003) Association of trypsin expression with tumour progression and matrilysin expression in human colorectal cancer. J Pathol 199: 176–184
5. Lin XY, Zhu ZM, Zhao CF, Li SG, Liu QC, Liu AL, Lin LQ, Lin XH (2019) Robust oxidase mimicking activity of protamine-stabilized platinum nanoparticles units and applied for colorimetric sensor of trypsin and inhibitor. Sensor Actuat B-Chem 284:346–353
6. Zaccheo BA, Crooks RM (2011) Self-powered sensor for naked-eye detection of serum trypsin. Anal Chem 83:1185–1188
7. Liu RX, Tan Y, Zhang CL, Wu JT, Mei L, Jiang YY, Tan CY (2013) A real-time fluorescence turn-on assay for trypsin based on a conjugated polyelectrolyte. J Mater Chem B 1:1402–1405
8. Yan XW, Yang LM, Wang QQ (2011) Lanthanide-coded protease-specific peptide-nanoparticle probes for a label-free multiplex protease assay using element mass spectrometry: a proof-of-concept study. Angew Chem Int Ed 50:5130–5133
9. Lu W, Jin Y, Wang G, Chen D, Li J (2008) Enhanced photoelectrochemical method for linear DNA hybridization detection using Au-nanopaticle labeled DNA as probe onto titanium dioxide electrode. Biosens Bioelectron 23:1534–1539
10. Zhao Y, Gong J, Zhang XB, Kong RM, Qu FL (2018) Enhanced biosensing platform constructed using urchin-like ZnO-Au@CdS microspheres based on the combination of photoelectrochemical and bioetching strategies. Sensor Actuat B-Chem 255:1753–1761
11. Zang Y, Lei J, Ju H (2017) Principles and applications of photoelectrochemical sensing strategies based on biofunctionalized nanostructures. Biosens Bioelectron 96:8–16
12. Fan D, Guo C, Ma H, Zhao D, Li Y, Wu D, Wei Q (2016) Facile fabrication of an aptasensor for thrombin based on graphitic carbon nitride/TiO_2 with high visible-light photoelectrochemical activity. Biosens Bioelectron 75:116–122
13. Komathi S, Muthuchamy N, Lee KP, Gopalan AI (2016) Fabrication of a novel dual mode cholesterol biosensor using titanium dioxide nanowire bridged 3D graphene nanostacks. Biosens Bioelectron 84:64–71
14. Huang Q, Chen H, Xu L, Lu D, Tang L, Jin L, Xu Z, Zhang W (2013) Visible-light-activated photoelectrochemical biosensor for the study of acetylcholinesterase inhibition induced by endogenous neurotoxins. Biosens Bioelectron 45:292–299
15. Pan K, Zhang Q, Wang Q, Liu Z, Wang D, Li J, Bai Y (2007) The photoelectrochemical properties of dye-sensitized solar cells made with TiO_2 nanoribbons and nanorods. Thin Solid Films 515:4085–4091
16. Sun WT, Yu Y, Pan HY, Gao XF, Chen Q, Peng LM (2008) CdS quantum dots sensitized TiO_2 nanotube-array photoelectrodes. J Am Chem Soc 130:1124–1125
17. Zhang H, Wang G, Chen D, Lv X, Li J (2008) Tuning photoelectrochemical performances of Ag-TiO_2 nanocomposites via reduction/oxidation of Ag. Chem Mater 20:6543–6549
18. Li Z, Qu Y, He G, Humayun M, Chen S, Jing L (2015) Enhanced visible-light activities for PEC water reduction of CuO nanoplates by coupling with anatase TiO_2 and mechanism. Appl Surf Sci 351: 681–685
19. Han M, Jia J (2016) 3D Bi_2S_3/TiO_2 cross-linked heterostructure: an efficient strategy to improve charge transport and separation for high photoelectrochemical performance. J Power Sources 32:923–930
20. Çakıroğlua B, Özacar M (2018) A self-powered photoelectrochemical glucose biosensor based on supercapacitor Co_3O_4-CNT hybrid on TiO_2. Biosens Bioelectron 119:34–41
21. Guo KY, Liu ZF, Han JH, Liu ZC, Li YJ, Wang B, Cui T, Zhou CL (2014) Hierarchical TiO_2–$CuInS_2$ core–shell nanoarrays for photoelectrochemical water splitting. Phys Chem Chem Phys 16: 16204–16213
22. Zhang G, Liu H, Qu J, Li J (2016) Two-dimensional layered MoS_2: rational design, properties and electrochemical applications. Energy Environmen Sci 9:1190–1209
23. Liu XQ, Huo XH, Liu PP, Tang YF, Xu J, Liu XH, Zhou YM (2017) Assembly of MoS_2 nanosheet-TiO_2 nanorod heterostructure as sensor scaffold for photoelectrochemical biosensing. Electrochim Acta 242:327–336
24. Lukowski MA, Daniel AS, Meng F, Forticaux A, Li L, Jin S (2013) Enhanced hydrogen evolution catalysis from chemically exfoliated metallic MoS_2 nanosheets. J Am Chem Soc 135:10274–10277
25. Meng F, Li J, Cushing SK, Zhi M, Wu N (2013) Solar hydrogen generation by nanoscale p–n junction of p-type molybdenum disulfide/n-type nitrogen-doped reduced graphene oxide. JAm ChemSoc 135:10286–10289
26. Mak KF, Lee C, Hone J, Shan J, Heinz TF (2010) Atomically thin MoS_2: a new directgap semiconductor. Phys Rev Lett 105:136805
27. Wang L, Wang C, Liu W, Chen Q, He M (2016) Visible-light-induced aerobic thiocyanation of indoles using reusable TiO_2/MoS_2 nanocomposite photocatalyst. Tetrahedron Lett 57:1771–1774
28. Du T, Wang N, Chen H, He H, Lin H, Liu K (2015) TiO_2-based solar cells sensitized by chemical-bath-deposited few-layer MoS_2. J Power Sources 275:943–949
29. Scalise E, Houssa M, Pourtois G, Afanas'ev V, Stesmans A (2012) Strain-induced semiconductor to metal transition in the two-dimensional honeycomb structure of MoS_2. Nano Res 5:43–48
30. Liu C, Wang L, Tang Y, Luo S, Liu Y, Zhang S, Zeng Y, Xu Y (2015) Vertical single or few-layer MoS_2 nanosheets rooting into

TiO_2 nanofibers for highly efficient photocatalytic hydrogen evolution. Appl Catal B 164:1–9

31. Liu X, Xing Z, Zhang Y, Li Z, Wu X, Tan S, Yu X, Zhu Q, Zhou W (2017) Fabrication of 3D flower-like black N-TiO_{2-x}@MoS_2 for unprecedented-high visible-light driven photocatalytic performance. Appl Catal B 201:119–127
32. Yang Z, Jian Z, Chen X, Li J, Qin P, Zhao J, Jiao XA, Hu X (2015) Electrochemical impedance immunosensor for sub-picogram level detection of bovine interferon gamma based on cylinder-shaped TiO_2 nanorods. Biosens Bioelectron 63:190–195
33. Guo B, Yu K, Fu H, Hua Q, Qi R, Li H, Song H, Guo S, Zhu Z (2015) Firework-shaped TiO_2 microspheres embedded with few-layer MoS_2 as an anode material for excellent performance lithium-ion batteries. J Mater Chem A 3:6392–6401
34. Lang D, Shen TT, Xiang QJ (2015) Roles of MoS_2 and graphene as cocatalysts in the enhanced visible-light photocatalytic H_2 production activity of multiarmed CdS nanorods. Chem Cat Chem 7:943–951
35. Borgström A, Andren-Sandberg A (1995) Elevated serum levels of immunoreactive anionic trypsin (but not cationic trypsin) signals pancreatic disease. Int J Pancreatol 18:221–225